A Generalized Navigation Correction Method for Airborne Doppler Radar Data

HUAQING CAI,[a] WEN-CHAU LEE,[b] MICHAEL M. BELL,[c] CORY A. WOLFF,[b] XIAOWEN TANG,[d] AND FRANK ROUX[e]

[a] *U.S. Army Research Laboratory, White Sands Missile Range, New Mexico*
[b] *National Center for Atmospheric Research, Boulder, Colorado*
[c] *Colorado State University, Fort Collins, Colorado*
[d] *School of Atmospheric Sciences, Nanjing University, Nanjing, China*
[e] *Laboratoire d'Aérologie, Université de Toulouse, and CNRS, Toulouse, France*

(Manuscript received 20 February 2018, in final form 30 May 2018)

ABSTRACT

Uncertainties in aircraft inertial navigation system and radar-pointing angles can have a large impact on the accuracy of airborne dual-Doppler analyses. The Testud et al. (THL) method has been routinely applied to data collected by airborne tail Doppler radars over flat and nonmoving terrain. The navigation correction method proposed in Georgis et al. (GRH) extended the THL method over complex terrain and moving ocean surfaces by using a variational formulation but its capability over ocean has yet to be tested. Recognizing the limitations of the THL method, Bosart et al. (BLW) proposed to derive ground speed, tilt, and drift errors by statistically comparing aircraft in situ wind with dual-Doppler wind at the flight level. When combined with the THL method, the BLW method can retrieve all navigation errors accurately; however, it can be applied only to flat surfaces, and it is rather difficult to automate. This paper presents a generalized navigation correction method (GNCM) based on the GRH method that will serve as a single algorithm for airborne tail Doppler radar navigation correction for all possible surface conditions. The GNCM includes all possible corrections in the cost function and implements a new closure assumption by taking advantage of an accurate aircraft ground speed derived from GPS technology. The GNCM is tested extensively using synthetic airborne Doppler radar data with known navigation errors and published datasets from previous field campaigns. Both tests show the GNCM is able to correct the navigation errors associated with airborne tail Doppler radar data with adequate accuracy.

1. Introduction

Airborne Doppler radars have played a key role in recent years for studying various weather phenomena, including supercells, frontal systems, drylines, squall lines, mesoscale convective systems, and hurricanes (e.g., Marks et al. 1992; Jorgensen et al. 1997; Wakimoto et al. 1998; Chong and Bousquet 1999; Wakimoto and Cai 2002; Cai et al. 2006; Reasor et al. 2009; Wakimoto and Murphey 2009; Cai and Lee 2013; Guy and Jorgensen 2014; Tang et al. 2014). The processing of airborne Doppler radar data poses an extra challenge compared with that of ground-based radars owing to the fact that radars are mounted on a moving platform (i.e., an aircraft). Hence, precisely removing the platform motion components from the measured Doppler velocities and mapping radar data onto an Earth-relative coordinate system are imperative steps to produce an accurate dual-Doppler wind synthesis (Lee et al. 1994, 2003; Testud et al. 1995, hereafter THL).

In addition to proper navigation correction, airborne tail Doppler radar data also require careful data quality control (QC) to remove all the spurious nonweather echoes before any meaningful dual-Doppler analysis can be carried out. Both navigation correction and airborne radar data QC processes used to be complex, tedious, and time-consuming tasks that could be performed only after each field campaign by a handful of radar experts (e.g., Jorgensen et al. 1997; Wakimoto et al. 2004). Recently, the automated QC package of airborne Doppler radar data was presented by Bell et al. (2013). This paper presents a

Corresponding author: Dr. Huaqing Cai, huaqing.cai.civ@mail.mil

DOI: 10.1175/JTECH-D-18-0028.1

generalized and automated navigation correction algorithm. The combination of the automated data QC and navigation correction procedures 1) offers the possibility to implement a real-time dual-Doppler synthesis algorithm on board a research aircraft, a desirable capability that is essential to mission execution and crew safety during airborne campaigns in the future; and 2) significantly reduces the time and efforts needed to deduce research-quality dual-Doppler winds in research mode.

For the National Center for Atmospheric Research (NCAR) Electra Doppler Radar (ELDORA; Hildebrand et al. 1996) and the National Oceanic and Atmospheric Administration (NOAA) P3 tail Doppler radars (TDR; Guy and Jorgensen 2014), there are a total of nine parameters involved in calculating the platform motion components and the coordinate transformation to map airborne radar data onto an Earth-relative coordinate system. Among the nine parameters, four of them are related to aircraft angles (i.e., heading, drift, pitch, and roll), two of them are related to aircraft speed (i.e., aircraft ground speed and vertical velocity), two of them are related to radar mounting and pointing (i.e., tilt and rotation), and one of them is related to radar hardware (i.e., range delay). The errors associated with these nine parameters result from the uncertainty in the aircraft inertial navigation system (INS), mounting and calibration errors in the radar system, the physical separation between the INS and radar antenna, flexibility (distortion) of the airframe, and other unknown random error sources (Lee et al. 1994; Bosart et al. 2002, hereafter BLW). Assuming Earth's surface is flat and stationary, THL developed a systematic method to derive all the navigation errors in two variational equations except the tilt error, which was assumed to be known or negligible. The THL method became a routine procedure for processing NCAR ELDORA and NOAA TDR data.

Recognizing the THL method can be applied only to a flat and stationary surface, Georgis et al. (2000, hereafter GRH) combined the two variational equations in the THL method into a single variational equation to compute airborne Doppler radar navigation corrections by employing a digital terrain map (DTM). The GRH method improved upon the THL method by removing the assumption of a flat Earth surface, therefore allowing the method to be applied over any terrain. Just like the original THL method, the GRH method also assumed the tilt errors were negligible. Moreover, the rotation/roll correction was assumed the same for both fore and aft radars, which is usually not true based on data from previous field projects (THL; BLW). The GRH method also included a cost function based on the difference between flight-level in situ wind and single-Doppler velocity near aircraft at the flight level, but its capability for deriving navigation corrections over a moving surface (i.e., ocean) has yet to be fully tested. The GRH method reduces to the THL method when the surface is flat and when the in situ wind constraint and horizontal aircraft position errors are not considered.

To retrieve navigation corrections over a moving surface, BLW developed a method to derive navigation corrections by satisfying three criteria: First, the in situ winds are statistically consistent with the dual-Doppler winds near the aircraft at the flight level; second, the flight-level dual-Doppler winds across the flight track are continuous (i.e., the wind speed and direction are statistically consistent across the flight track); and third, the residual surface Doppler velocity in the fore radar should have approximately the same magnitude but opposite sign as the aft radar on the opposite side of the plane. The BLW method has been successfully applied to ELDORA data in a number of field campaigns over ocean (e.g., Wakimoto and Bosart 2001; Bell and Montgomery 2010). However, the method can be used only when there is enough radar echo near the aircraft for dual-Doppler synthesis and when the aircraft is over a flat surface. The process requires manually running the following algorithms/steps multiple times until the three criteria discussed above were met: 1) perform dual-Doppler synthesis near the aircraft, 2) compute the statistics of the differences between dual-Doppler winds and in situ winds, and 3) estimate and apply the corrections of tilt/ground speed based on the statistics obtained from step 2. The whole process is labor intensive and is difficult to automate for real-time applications in its current form.

The goal of this paper is to present a generalized navigation correction method (GNCM) based on the GRH framework and 1) include tilt corrections for fore and aft radars as independent parameters, 2) differentiate rotation/roll corrections for fore and aft radars as independent parameters, and 3) work over any surface conditions (i.e., flat terrain, complex terrain, and ocean). The GNCM assumes the much more accurate aircraft ground speed derived from the GPS information as known to close the previously underdetermined systems in THL, GRH, and BLW. The GNCM has been tested thoroughly using synthetic ELDORA data with known navigation errors and real ELDORA data from previous field campaigns. It can replace the THL, GRH, and

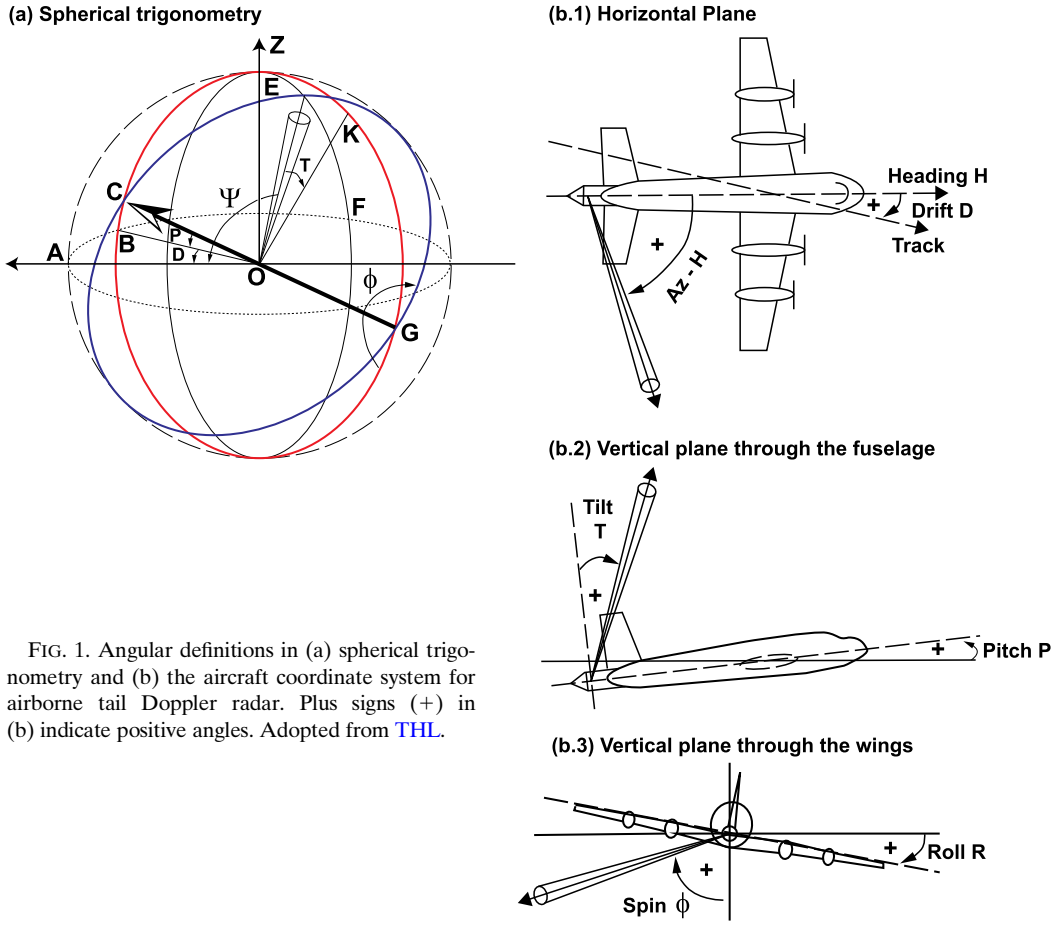

FIG. 1. Angular definitions in (a) spherical trigonometry and (b) the aircraft coordinate system for airborne tail Doppler radar. Plus signs (+) in (b) indicate positive angles. Adopted from THL.

BLW algorithms, and serve as a single unified algorithm for airborne tail Doppler radar navigation correction.

The paper is organized as follows. Section 2 provides a brief review of the GRH method and GNCM formulation. Sections 3 and 4 present test results of the GNCM using synthetic airborne Doppler radar data and previous field campaign data from NCAR ELDORA, respectively. A discussion on how to best utilize GNCM and a summary are given in section 5.

2. The GNCM

a. *Definition of angles*

Before the detailed formulation of GNCM is presented in the next section, a general description of the angle definitions used in airborne tail Doppler radar navigation correction is given herein for the convenience of the reader of this paper, although similar descriptions have been presented elsewhere (e.g., THL; Guy and Jorgensen 2014).

Figure 1, which is adopted from THL, illustrates the angular definition in both spherical trigonometry (Fig. 1a) and aircraft coordinate system (Fig. 1b). The notions in Fig. 1 can be divided into several groups as follows:

1) General description
   - *O* is the position of the radar antenna and the center of a reference sphere (dashed circle in Fig. 1a).
   - *Z* is the zenith of the reference sphere.
   - All circles in Fig. 1a are great circles.
2) Aircraft coordinates
   - *C* (*G*) is the intersection of the nose (tail) of the fuselage and the reference sphere. *CG* is along the aircraft fuselage, which is also the antenna spin axis.
   - *OB* (the aircraft heading) is the projection of *OC* to the horizontal plane (the dotted black circle).

- A is the intersection of the aircraft track velocity and the reference sphere (i.e., OA is the track).
- K is the vertical with respect to the aircraft fuselage ($CO \perp KO$). The red great circle passes through C, K, and G.
- Angle D (arc AB) is the drift, which is defined as the angle from the vertical plane, including the antenna spin axis (heading) to the horizontal component of the aircraft velocity (track). The drift is positive if the track is more clockwise than the heading.
- Angle P (arc BC) is the pitch of the antenna spin axis (positive up).

3) Absolute beam coordinates
   - E is the intersection of the radar beam and the reference sphere. The blue circle passes through C, E, and G, while the black circle is in a vertical plane passing through E. Point F is one of the intersections of the black circle and the horizontal plane (the dotted black circle).
   - Arc EF is the elevation angle of the beam with respect to the horizontal plane.
   - Ψ (arc EA) is the angle between the beam and the horizontal component of aircraft velocity (track OA).
4) Beam coordinates relative to the aircraft
   - Angle T is the tilt from the plane perpendicular to the spin axis to the beam. Tilt is positive (negative) when antenna is pointing fore (aft).
   - Angle ϕ is the spin (the sum of the radar rotation angle given by the encoder and the roll of the aircraft). Both spin and rotation angles are measured clockwise when looking forward. A zero rotation angle corresponds to the antenna pointed downward with respect to the aircraft, while a zero spin angle corresponds to a beam pointed toward nadir.
   - Azimuth angle A_Z (arc BF) is the azimuth of the beam relative to heading (positive clockwise).

Similarly, Fig. 1b illustrates heading, drift, and azimuth angles in Fig. 1b(1); pitch and tilt in Fig. 1b(2); and spin and roll in Fig. 1b(3) in the aircraft coordinate system.

b. Formulation of the GNCM

The goal of this paper is to develop a single algorithm that can be used over any surface (i.e., flat, complex terrain, or ocean) and applied to any airborne tail Doppler radar. The GNCM provides the possibility of replacing the THL, GRH, and BLW methods to serve as the one single algorithm that could handle all surface conditions. It expands on the GRH method and includes additional variables for a better representation of the possible biases. The GRH method was formulated as the minimization of a cost function resulting from the normalized sum of three contributions—J_1, J_2, and J_3—with respect to nine unknown corrections in aircraft and radar attitude angles (roll/rotation ΔR, heading/drift ΔH, pitch ΔP), horizontal aircraft speed ΔV, aircraft location (eastward Δx, northward Δy, upward Δz), and radar range delay (Δd_f and Δd_a for the fore and aft radars, respectively). Since aircraft roll and rotation corrections are defined on the same axis, the two corrections are inseparable and have been combined into a single rotation correction. The same argument can also be applied to heading and drift corrections; as a result, heading and drift corrections have been combined into a single heading correction. However, the GRH method unnecessarily assumed the tilt angle corrections (ΔT_f and ΔT_a) were zero and the rotation angle corrections (ΔR_a and ΔR_f) were the same for both fore and aft tilts, which is not always true (BLW). Therefore, the GNCM adds the tilt angle corrections and the individual rotation angle corrections for the fore and aft tilts, respectively.

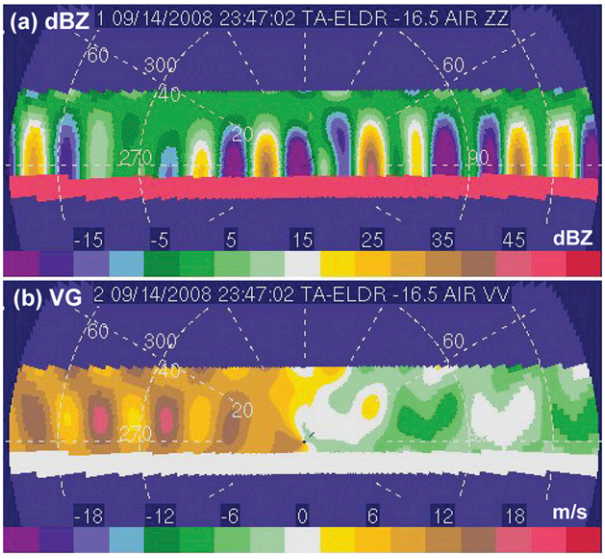

FIG. 2. An example of synthetic ELDORA data. (a) Radar reflectivity; and (b) ground-relative single-Doppler velocity. The aircraft was at 3 km AGL. The surface is flat.

Similar to the GRH method [see their Eq. (1)], J_1 is a cost function quantifying the difference between radar-derived surface altitude $z_{\mathrm{RAD}}(n)$ and DTM-derived altitude at the same horizontal location $h_{\mathrm{DTM}}[x_{\mathrm{RAD}}(n), y_{\mathrm{RAD}}(n)]$, after adding the variations of z_{RAD} and h_{DTM} because of navigation errors:

$$J_1 = \sum_{n=1}^{N_{\mathrm{SURF}}} \mu_{\mathrm{SURF}}(n) \left(\begin{bmatrix} z_{\mathrm{RAD}}(n) + \frac{\partial z_{\mathrm{RAD}}}{\partial P}(n)\Delta P + \frac{\partial z_{\mathrm{RAD}}}{\partial H}(n)\Delta H + \frac{\partial z_{\mathrm{RAD}}}{\partial d_f}(n)\Delta d_f \\ + \frac{\partial z_{\mathrm{RAD}}}{\partial T_f}(n)\Delta T_f + \frac{\partial z_{\mathrm{RAD}}}{\partial R_f}(n)\Delta R_f + \frac{\partial z_{\mathrm{RAD}}}{\partial d_a}(n)\Delta d_a \\ + \frac{\partial z_{\mathrm{RAD}}}{\partial T_a}(n)\Delta T_a + \frac{\partial z_{\mathrm{RAD}}}{\partial R_a}(n)\Delta R_a + \frac{\partial z_{\mathrm{RAD}}}{\partial V}(n)\Delta V + \Delta z \end{bmatrix} - \left\{ \begin{array}{c} h_{\mathrm{DTM}}[x_{\mathrm{RAD}}(n), y_{\mathrm{RAD}}(n)] \\ + \frac{\partial h_{\mathrm{DTM}}}{\partial x_{\mathrm{RAD}}} \begin{bmatrix} \frac{\partial x_{\mathrm{RAD}}}{\partial P}(n)\Delta P + \frac{\partial x_{\mathrm{RAD}}}{\partial H}(n)\Delta H + \frac{\partial x_{\mathrm{RAD}}}{\partial d_f}(n)\Delta d_f \\ + \frac{\partial x_{\mathrm{RAD}}}{\partial T_f}(n)\Delta T_f + \frac{\partial x_{\mathrm{RAD}}}{\partial R_f}(n)\Delta R_f + \frac{\partial x_{\mathrm{RAD}}}{\partial d_a}(n)\Delta d_a \\ + \frac{\partial x_{\mathrm{RAD}}}{\partial T_a}(n)\Delta T_a + \frac{\partial x_{\mathrm{RAD}}}{\partial R_a}(n)\Delta R_a + \frac{\partial x_{\mathrm{RAD}}}{\partial V}(n)\Delta V + \Delta x \end{bmatrix} \\ + \frac{\partial h_{\mathrm{DTM}}}{\partial y_{\mathrm{RAD}}} \begin{bmatrix} \frac{\partial y_{\mathrm{RAD}}}{\partial P}(n)\Delta P + \frac{\partial y_{\mathrm{RAD}}}{\partial H}(n)\Delta H + \frac{\partial y_{\mathrm{RAD}}}{\partial d_f}(n)\Delta d_f \\ + \frac{\partial y_{\mathrm{RAD}}}{\partial T_f}(n)\Delta T_f + \frac{\partial y_{\mathrm{RAD}}}{\partial R_f}(n)\Delta R_f + \frac{\partial y_{\mathrm{RAD}}}{\partial d_a}(n)\Delta d_a \\ + \frac{\partial y_{\mathrm{RAD}}}{\partial T_a}(n)\Delta T_a + \frac{\partial y_{\mathrm{RAD}}}{\partial R_a}(n)\Delta R_a + \frac{\partial y_{\mathrm{RAD}}}{\partial V}(n)\Delta V + \Delta y \end{bmatrix} \end{array} \right\} \right)^2, \quad (1)$$

where N_{SURF} is the number of gates affected by surface in a ray (referred to as surface gates or surface echoes); $\mu_{\mathrm{SURF}}(n)$ is a weight proportional to the surface reflectivity and its gradient; and the values of partial derivatives of x_{RAD}, y_{RAD}, and z_{RAD} with respect to aircraft roll/rotation, pitch, drift/heading, tilt, and radar range delay for each surface gate n are obtained from simple geometry as shown in the appendix of GRH. For the method of how the surface gates and their associated weights were determined, the reader is referred to GRH for further details.

Cost function J_2 deals with the Doppler velocity of the surface echoes V_{SURF}, which is assumed to be zero if there were no navigation errors (i.e., nonmoving surface). The J_2 term characterizes variations of surface echo velocity caused by navigation errors:

$$J_2 = \sum_{n=1}^{N_{\mathrm{SURF}}} \mu_{\mathrm{SURF}}(n) \left\{ \begin{bmatrix} V_{\mathrm{SURF}}(n) + \frac{\partial V_{\mathrm{SURF}}}{\partial P}(n)\Delta P + \frac{\partial V_{\mathrm{SURF}}}{\partial H}(n)\Delta H + \frac{\partial V_{\mathrm{SURF}}}{\partial T_f}(n)\Delta T_f \\ + \frac{\partial V_{\mathrm{SURF}}}{\partial T_a}(n)\Delta T_a + \frac{\partial V_{\mathrm{SURF}}}{\partial R_f}(n)\Delta R_f + \frac{\partial V_{\mathrm{SURF}}}{\partial R_a}(n)\Delta R_a \\ + \frac{\partial V_{\mathrm{SURF}}}{\partial V}(n)\Delta V \end{bmatrix} \right\}^2, \quad (2)$$

where the values of the partial derivatives of V_{SURF} with respect to aircraft roll/rotation, pitch, drift/heading, tilt, and ground speed for each surface gate n are derived from geometry in the same manner as in J_1.

Cost function J_3 deals with the N_{NEAR} differences between the single-Doppler velocity V_{NEAR} from the radar and the projection of the in situ wind $V_{\mathrm{IN\ SITU}}$ along the radar beam, after adding the variations caused by aircraft altitude angle and speed errors:

$$J_3 = \sum_{n=1}^{N_{\mathrm{NEAR}}} \mu_{\mathrm{NEAR}}(n) \left\{ \left[V_{\mathrm{NEAR}}(n) + \frac{\partial V_{\mathrm{NEAR}}}{\partial P}(n)\Delta P + \frac{\partial V_{\mathrm{NEAR}}}{\partial H}(n)\Delta H + \frac{\partial V_{\mathrm{NEAR}}}{\partial T_f}(n)\Delta T_f + \frac{\partial V_{\mathrm{NEAR}}}{\partial T_a}(n)\Delta T_a + \frac{\partial V_{\mathrm{NEAR}}}{\partial R_f}(n)\Delta R_f + \frac{\partial V_{\mathrm{NEAR}}}{\partial R_a}(n)\Delta R_a + \frac{\partial V_{\mathrm{NEAR}}}{\partial V}(n)\Delta V \right] - \left[V_{\mathrm{INSITU}}(n) + \frac{\partial V_{\mathrm{INSITU}}}{\partial P}(n)\Delta P + \frac{\partial V_{\mathrm{INSITU}}}{\partial H}(n)\Delta H + \frac{\partial V_{\mathrm{INSITU}}}{\partial T_f}(n)\Delta T_f + \frac{\partial V_{\mathrm{INSITU}}}{\partial T_a}(n)\Delta T_a + \frac{\partial V_{\mathrm{INSITU}}}{\partial R_f}(n)\Delta R_f + \frac{\partial V_{\mathrm{INSITU}}}{\partial R_a}(n)\Delta R_a + \frac{\partial V_{\mathrm{INSITU}}}{\partial V}(n)\Delta V \right] \right\}^2, \tag{3}$$

where $\mu_{\mathrm{NEAR}}(n)$ is a weight inversely proportional to the distance between the considered gate and the aircraft. The GRH method restricted the domain for V_{NEAR} and $V_{\mathrm{IN\ SITU}}$ within a wedge of low elevation ($<\pm 5°$) and close horizontal distance (<3 km). We will show in the next section that the range recommendation from GRH can be modified to yield better results, and the formulation of cost function J_3 does not require the radar measurement to be taken near the aircraft and at low elevations.

A solution for the navigation corrections is obtained through the minimization of the normalized sum of J_1, J_2, and J_3:

$$J = \frac{\delta_1 J_1}{\sum_1^{N_{\mathrm{SURF}}} \mu_{\mathrm{SURF}}(n) \| z_{\mathrm{RAD}}(n) - h_{\mathrm{DTM}}[x_{\mathrm{RAD}}(n), y_{\mathrm{RAD}}(n)] \|} + \frac{\delta_2 J_2}{\sum_1^{N_{\mathrm{SURF}}} \mu_{\mathrm{SURF}}(n) \| V_{\mathrm{SURF}}(n) \|} + \frac{\delta_3 J_3}{\sum_1^{N_{\mathrm{NEAR}}} \mu_{\mathrm{NEAR}}(n) \| [V_{\mathrm{NEAR}}(n) - V_{\mathrm{INSITU}}(n)] \|}, \tag{4a}$$

where symbol "||" denotes absolute values. Terms δ_1, δ_2, and δ_3 are either one or zero so that corresponding cost functions J_1, J_2, and J_3 can be either included or omitted in calculating J. Term J is minimized with respect to errors in roll/rotation, tilt, pitch, heading/drift, aircraft horizontal position, aircraft altitude, radar range delays, and aircraft ground speed, as

$$\frac{\partial J}{\partial(\Delta x, \Delta y, \Delta z, \Delta P, \Delta H, \Delta d_f, \Delta T_f, \Delta R_f, \Delta d_a, \Delta T_a, \Delta R_a, \Delta V)} = 0. \tag{4b}$$

A system of 12 linear equations can be obtained from such derivatives, which can be readily solved through the inversion of a 12×12 matrix. Notice Eqs. (1)–(4) are similar to Eqs. (1)–(4) in GRH except that tilt corrections for both fore and aft radars are added, and fore and aft rotation corrections are separated. By including tilt corrections for both antennas and an individual rotation angle of fore and aft tilts, a 9×9 system in GRH turns into a 12×12 system with 12 unknowns in this paper. For your convenience, a parameter list for GNCM can be found in appendix A.

As GRH pointed out, the formulation is equivalent to that used by THL when the surface is flat and when the

in situ data constraint and horizontal aircraft position errors are not considered. In other words, the generalized navigation correction formulation expands the THL method by adding complex terrain, aircraft horizontal position correction, and the in situ data constraint into three cost functions. The new generalized formulation improves upon the GRH method by adding tilt corrections and individual fore and aft rotation angle corrections. The new formulation improves upon the BLW method by removing the flat surface constraint and avoiding the cumbersome iterative processes used in that method. It is expected that GNCM could replace the THL, GRH, and BLW methods and can be applied to any kind of surface conditions. Moreover, since the formulation of the GNCM does not depend on a particular platform, it should be applicable to ELDORA, NOAA TDRs, and future scanning airborne Doppler radars.

3. Test of the GNCM using synthetic data

a. Closure assumptions of GNCM

According to THL, the rotation, pitch, range delay, and aircraft altitude corrections can be determined accurately solely based on a range constraint, while drift D, tilt T, and ground speed V_H corrections ΔD, ΔT, and ΔV, respectively, are determined from a set of two equations based on a surface velocity constraint over a flat and motionless surface:

$$A = -V_H \cos D \cos T \Delta T + \sin T (V_H \sin D \Delta D - \cos D \Delta V) \quad \text{and} \tag{5}$$

$$B_1 = -V_H \sin D \sin T \Delta T + \cos T (V_H \cos D \Delta D - \sin D \Delta V), \tag{6}$$

where A and B_1 are coefficients from the Fourier analysis obtained by the THL method using the antenna spin angle as an independent variable [see their Eqs. (10)–(12)]. Since there are three unknowns with two equations, the solution is underdetermined. To solve the above equations, closure assumptions have to be made. There are three options: 1) assume tilt error is known or negligible, then solve for heading and ground speed corrections; or 2) assume drift/heading error is known or negligible, then solve for tilt and ground speed corrections; or 3) assume ground speed error is known or negligible, then solve for tilt and heading/drift corrections.

For option 1, let $\Delta T = 0$ in Eqs. (5) and (6), then we have

$$A = \sin T (V_H \sin D \Delta D - \cos D \Delta V) \tag{7}$$

$$B_1 = \cos T (V_H \cos D \Delta D - \sin D \Delta V). \tag{8}$$

Transform the above equations into a matrix form of

$$\mathbf{MX} = \mathbf{N},$$

where

$$\mathbf{M} = \begin{bmatrix} V_H \sin T \sin D & -\sin T \cos D \\ V_H \cos T \cos D & -\cos T \sin D \end{bmatrix},$$

$$\mathbf{X} = \begin{bmatrix} \Delta D \\ \Delta V \end{bmatrix}, \quad \text{and} \quad \mathbf{N} = \begin{bmatrix} A \\ B_1 \end{bmatrix}.$$

This linear system has a unique solution for $\mathbf{X}$ if and only if the determinant of $\mathbf{M}$ denoted as $\mathrm{Det}(\mathbf{M}) = V_H \sin T \cos T (1 - 2\sin^2 D)$ is not zero. For ELDORA or NOAA TDR, $V_H = \sim 120\,\mathrm{m\,s^{-1}}$, $T = \sim \pm 18°$, then $V_H \sin T \cos T \neq 0$. Since $1 - 2\sin^2 D = 0$ when $D = \pm 45°$, we can conclude that except under the rare condition of drift $= \pm 45°$, option 1 will produce a unique solution for heading/drift and ground speed corrections based on Eqs. (7) and (8). This option was the approach used by THL and GRH. However, BLW showed that in general the tilt error is nonnegligible, but a similar direct solution can be derived if the tilt error is assumed to be known or can be estimated by another method.

Similarly, for option 2, let $\Delta D = 0$, then Eqs. (5) and (6) become

$$A = -V_H \cos D \cos T \Delta T - \sin T \cos D \Delta V \quad \text{and} \tag{9}$$

$$B_1 = -V_H \sin D \sin T \Delta T - \cos T \sin D \Delta V. \tag{10}$$

Then

$$\mathbf{M} = \begin{bmatrix} -V_H \cos D \cos T & -\sin T \cos D \\ -V_H \sin D \sin T & -\cos T \sin D \end{bmatrix},$$

$$\mathbf{X} = \begin{bmatrix} \Delta T \\ \Delta V \end{bmatrix}, \quad \text{and} \quad \mathbf{N} = \begin{bmatrix} A \\ B_1 \end{bmatrix},$$

and $\mathrm{Det}(\mathbf{M}) = V_H \sin D \cos D (1 - 2\sin^2 T)$. Since $V_H = \sim 120\,\mathrm{m\,s^{-1}}$, $T = \sim \pm 18°$, then $1 - 2\sin^2 T \neq 0$, and $\mathrm{Det}(\mathbf{M}) = 0$ when $D = 0°$ or $90°$. This means mathematically Eqs. (9) and (10) can be used to solve tilt and ground speed corrections if the drift angle is not zero. However, in practice, option 2 is not recommended for the following reasons: 1) According to THL, the statistical uncertainty of drift is the largest among all the angles. As a matter of fact, it is ~20 times larger than the statistical uncertainty of any other angles (~1° vs ~0.05°), which makes assuming no errors in drift/heading unrealistic. 2) As we will discuss in section 3, to obtain reliable results for navigation correction, straight and smooth calibration legs are recommended to mitigate turbulence effects. It is quite possible that this kind of flight pattern will also be associated with a near-zero

drift, which causes the solution of Eqs. (9) and (10) to be unstable because Det(**M**) approaches zero. This means that even if there are no drift/heading errors in the data, the algorithm still cannot determine tilt and ground speed corrections unambiguously when drift is sufficiently small. Therefore, option 2 is not a good assumption for solving the underdetermined linear system described by Eqs. (5) and (6).

Last, for option 3, let $\Delta V = 0$ in Eqs. (5) and (6), which yields

$$A = -V_H \cos D \cos T \Delta T + V_H \sin T \sin D \Delta D \quad \text{and} \tag{11}$$

$$B_1 = -V_H \sin D \sin T \Delta T + V_H \cos T \cos D \Delta D. \tag{12}$$

Again, solve the above equations using the matrix form where

$$\mathbf{M} = \begin{bmatrix} -V_H \cos D \cos T & V_H \sin T \sin D \\ -V_H \sin D \sin T & V_H \cos T \cos D \end{bmatrix},$$

$$\mathbf{X} = \begin{bmatrix} \Delta T \\ \Delta D \end{bmatrix}, \quad \text{and} \quad \mathbf{N} = \begin{bmatrix} A \\ B_1 \end{bmatrix}$$

and $\text{Det}(\mathbf{M}) = V_H^2(\sin^2 D - \cos^2 T)$. This linear system has a unique solution for **X** if $\sin D \neq \pm \cos T$. When $T = \sim \pm 18°$, this indicates that Eqs. (11) and (12) can be used to accurately retrieve heading/drift and tilt corrections when drift $D \neq \pm 72°$. Considering it is highly unlikely that the drift can be as large as $\pm 72°$ even if cross-track winds are as strong as category 4/5 hurricane winds, we can safely assume that option 3 will yield satisfactory retrievals of tilt and heading/drift corrections almost all the time. Though this option was not considered in the previous studies, neglecting the ground speed error proves to be an excellent option as described below. This option will be chosen as the closure assumption for GNCM based on various tests conducted in the next section.

b. *Test of GNCM under stationary surface condition*

The GNCM is written in FORTRAN and C languages and can be run by a single script. The users control the input parameters to the algorithm by a single text file. The ease of use of this algorithm is obvious compared with other methods, such as BLW, which requires users to manually rerun dual-Doppler synthesis several times until a satisfactory comparison between dual-Doppler winds and in situ winds is achieved. The code of the GNCM is part of the Lidar Radar Open Software Environment (LROSE) and can be obtained online (at https://nsf-lrose.github.io).

To fully test the effectiveness of the GNCM and various closure assumptions discussed above, a set of synthetic ELDORA data with known navigation errors was created. An example of the synthetic radar reflectivity and Doppler velocity is shown in Fig. 2. The surface is flat and the Doppler velocity field is prescribed as a Beltrami function (Shapiro et al. 2009). The flight track is a north–south track of ~35 km. The aircraft in situ winds are created by sampling the prescribed wind field along the flight track. Further details on the synthetic dataset are provided in appendix B.

For the purpose of testing the GNCM, we created three synthetic radar datasets according to the three options listed in the previous section, using typical navigation errors derived from previous field experiments, and ran the GNCM for each of them. Since the synthetic radar data have a flat, nonmoving surface, the DTM is simply a constant surface height. Note that the contribution from the in situ cost function J_3 in the case of a nonmoving surface is redundant, since cost function J_2 already provides the necessary velocity constraint. Therefore, the GNCM is run by using J_1 and J_2 cost functions only (the algorithm is flexible enough to let the users choose which terms of the cost function are included in the retrieval process). Tests using all three cost functions under a stationary surface condition yielded almost the same results as using cost function J_1 and J_2 (not shown). This is consistent with what GRH found in their paper. According to GRH, the surface height and velocity error reduction resultant from including J_3 is rather small, which suggests the impact of J_3 is limited when both J_1 and J_2 are utilized.

The true navigation errors and the retrieved corrections are shown in the upper part of Table 1, with the reduction of surface height and velocity errors for each option before and after navigation correction shown in the lower part of Table 1. It should be pointed out that since the retrieved navigation corrections are added back to the airborne Doppler data, a perfect retrieved result will have the same absolute values but opposite sign of the specified navigation errors in the synthetic data. In other words, when the sum of the true error and retrieved correction in Table 1 approaches zero, a fairly good retrieval is obtained. Clearly the GNCM was able to successfully retrieve the navigation corrections in the case of options 1 and 3, with accuracy within the limits provided by GRH (i.e., ~0.2°, ~20 m, and ~0.5 m s^{-1} for angles, altitude/range delay, and ground speed, respectively). Option 2 (neglecting drift error) yielded no results as expected, since drift was set to zero in the synthetic data, which would make Eqs. (9) and (10) have no solution. Consequently, option 2 is not considered further. The effect of navigation correction is best demonstrated in Table 1 by the significant reduction in the mean and standard deviation (STD) of the difference

TABLE 1. True errors and retrieved navigation corrections for the case of no tilt errors or no ground speed errors using synthetic ELDORA data under the condition of a stationary surface. Also shown in the lower part of the table are the mean and STD of DZ_{SURF} and V_{SURF} before and after the navigation correction was applied for the two cases.

	No tilt error	No ground speed error
	True error/retrieved correction	
Tilt aft (°)	—/—	0.3/−0.299
Tilt fore (°)	—/—	−0.3/0.300
Rotation/roll aft (°)	1.0/−0.999	1.0/−0.999
Rotation/roll fore (°)	2.0/−1.999	2.0/−1.999
Pitch (°)	1.5/−1.500	1.5/−1.500
Heading/drift (°)	0.5/−0.500	0.5/−0.500
Range delay aft (m)	150/−150.0	150/−150.0
Range delay fore (m)	200/−202.0	200/−202.0
Δx (m)	—/—	—/—
Δy (m)	—/—	—/—
Δz (km)	0.3/−0.299	0.3/−0.299
Ground speed ($m\,s^{-1}$)	1.0/−1.0	—/—
	Before → after correction	
Mean (STD) of DZ_{SURF} (km)	0.430 (0.183) → 0.001 (0.029)	0.426 (0.183) → 0.001 (0.029)
Mean (STD) of V_{SURF} ($m\,s^{-1}$)	1.942 (1.087) → −0.001 (0.001)	1.926 (1.198) → 0.000 (0.000)

between surface heights derived from radar and DTM (DZ_{SURF}), as well as by the mean and STD of surface velocity (V_{SURF}) literally approaching zero. This set of tests confirms the effectiveness of Eqs. (5) and (6) when closure option 1 or 3 was applied.

We have shown, both theoretically and numerically, that heading/drift, tilt, and ground speed errors cannot be determined unambiguously unless one of those errors is negligible or known. In real data, all three errors could be present at the same time, thus requiring further assumptions. Both THL and GRH used the same approximation by assuming the tilt error is zero based on the radar manufacturer's specification, which indicated the tilt errors should be small.[1] However, experiences from previous experiments and results from the enhanced THL (ETHL) method (BLW) suggested that tilt errors were larger than the manufacturer's specifications and are not negligible in general. The ETHL method makes use of asymmetries in the residual surface velocities to try to separate the tilt, drift, and ground speed error. However, since the problem is underdetermined, there can be multiple solutions that reduce the residual velocity to zero. Moreover, the ETHL algorithm requires a flat and stationary surface. Since there is no easy way to determine what the real tilt error is in a radar, the assumption of zero tilt error is difficult to justify. Instead of assuming zero tilt error as in previous navigation correction algorithms, an alternative approach we propose in this paper is to assume the ground speed error is zero. This method is novel and has several advantages. First, the ground speed error has already become smaller and will continue to decrease with the advancement of GPS technology. According to a U.S. government website providing information regarding current and future GPS technology (www.gps.gov), the GPS position error was ~3 m before 2010. Since all past ELDORA field projects were conducted before 2010, this means the accuracy of GPS-corrected ground speed for ELDORA was determined by the GPS position error of ~3 m. The position error has been reduced to ~1.5 m since the launch of GPS Block IIF satellites since 2010, and it will continue to decrease to ~0.63 m after the launch of GPS III satellites starting 2016 (see www.gps.gov). Thus, it is reasonable to anticipate the aircraft ground speed error derived from GPS measurement, which is directly related to GPS position error, will also continue to decrease by a factor of 2–4 from the current value of ~0.2 $m\,s^{-1}$. Second, experiences from previous field projects suggest that ground speed errors rarely exceed 1 $m\,s^{-1}$ (e.g., BLW). Finally, unlike tilt errors, the ground speed error has a secondary effect on dual-Doppler winds (see BLW, their Fig. 6). Therefore, the assumption of zero ground speed error will have less impact on dual-Doppler synthesis than assuming zero tilt error.

For the purpose of comparing how the GNCM performs under zero tilt error and zero ground speed error assumptions, we created a set of synthetic ELDORA data with a ground speed error of 1 $m\,s^{-1}$; a tilt error of

[1] THL assumed that only the tilt error was negligible for the French antennas used in ELDORA and one of the NOAA P3s. They did present a formula to estimate the tilt error for the mechanically scanning P3 antenna but that formula is not generally applicable.

TABLE 2. True errors and retrieved navigation corrections assuming no tilt errors or no ground speed errors for a case with tilt, heading, and ground speed errors specified in the synthetic data under the condition of a stationary surface. Also shown in the lower part of the table are the mean and STD of DZ_{SURF} and V_{SURF} before and after the navigation correction was applied for both assumptions.

	Assuming no tilt error	Assuming no ground speed error
	True error/retrieved correction	
Tilt aft (°)	0.3/—	0.3/−0.159
Tilt fore (°)	−0.3/—	−0.3/0.168
Rotation/roll aft (°)	1.0/−0.999	1.0/−0.999
Rotation/roll fore (°)	2.0/−1.999	2.0/−1.999
Pitch (°)	1.5/−1.487	1.5/−1.500
Heading/drift (°)	0.5/−0.500	0.5/−0.500
Range delay aft (m)	150/−150.0	150/−150.0
Range delay fore (m)	200/−203.0	200/−203.0
Δx (m)	—/—	—/—
Δy (m)	—/—	—/—
Δz (km)	0.3/−0.295	0.3/−0.298
Ground speed ($m\,s^{-1}$)	1.0/1.22	1.0/—
	Before → after correction	
Mean (STD) of DZ_{SURF} (km)	0.426 (0.183) → −0.000 (0.029)	0.426 (0.183) → 0.000/0.029
Mean (STD) of V_{SURF} ($m\,s^{-1}$)	1.937 (1.098) → −0.002 (0.007)	1.937 (1.098) → 0.000 (0.000)

0.3° and −0.3° for aft and fore radars, respectively; and a heading error of 0.5°. This set of synthetic radar data should mimic the real airborne Doppler radar data with typical navigation errors in aircraft angles, altitude, and ground speed (THL; BLW). We ran the GNCM using the zero tilt error and zero ground speed error assumptions, with the difference from the previous tests being that the synthetic data now contain all three errors (i.e., heading/drift, tilt, and ground speed), while in the previous section, the synthetic data contain only two errors (i.e., either heading/drift and ground speed or heading/drift and tilt). The results of the retrieved navigation corrections compared with the true errors are shown in the upper part of Table 2, and the reduction of surface height and velocity errors before and after navigation correction is shown in the lower part of Table 2. Notice in Table 2 that in the case of assuming no tilt errors, the retrieved ground speed error was off by ~2.22 $m\,s^{-1}$ (1.00 + 1.22 $m\,s^{-1}$), which is much larger than the accuracy of ground speed retrievals for the algorithm (i.e., 0.5 $m\,s^{-1}$ based on GRH). On the other hand, in the case of assuming no ground speed errors, the retrieved tilt errors of approximately −0.132° (−0.3° + 0.168°) and 0.141° (0.3° − 0.159°) are within the ~0.2° accuracy of the method. This suggests that a 1 $m\,s^{-1}$ ground speed error, which is typical based on past field project data, will produce a tilt error that is small enough that it may not be resolved by the GNCM. Also note that the mean and STD of surface echo velocity were reduced to near zero by the GNCM (see Table 2) in both cases, which confirms that there are multiple solutions to satisfy the cost function equally well mathematically. However, physically, ignoring ground speed error seems to be a better choice based on results from Table 2.

For the purpose of testing what magnitude of ground speed errors are acceptable to neglect using the GNCM, three more sets of synthetic ELDORA data with the same aircraft and INS errors as in Table 2 but different ground speed errors of 0.2, 0.5, and 1.5 $m\,s^{-1}$ were created. The GNCM algorithm was applied to the dataset assuming no ground speed errors. The true errors and retrieved navigation corrections are shown in the upper part of Table 3, and the reduction of surface height and velocity errors before and after navigation correction is shown in the lower part of Table 3. Table 3 clearly suggests that a smaller ground speed error yields a more accurate tilt correction retrieval. The retrieved tilt correction errors decreased by an order of magnitude from ~0.200° to ~0.028° when ground speed errors decreased from 1.5 to 0.2 $m\,s^{-1}$. This test offers hope to very accurately retrieve tilt errors when even more accurate aircraft ground speed is obtained in the future by improved GPS technology. Also note in Table 3 that the mean and STD of surface echo velocity were all very close to zero after correction factors were applied, which again confirms that the GNCM will create a set of solutions that mathematically satisfies the surface velocity cost function regardless of its physical meaning.

Based on the results of the synthetic ELDORA data test, we propose to assume zero ground speed error instead of zero tilt error when retrieving airborne Doppler radar navigation errors. This recommendation is different from previous practice using the THL, GRH, and BLW methods, but the preceding tests indicate it is more accurate and that accuracy should improve as

TABLE 3. True errors and retrieved navigation corrections assuming no ground speed errors for three cases with the same navigation errors except different ground speed specified in the synthetic data under the condition of a stationary surface. Also shown in the lower part of the table are the mean and STD of DZ_{SURF} and V_{SURF} before and after the navigation correction was applied for the three assumptions.

	Ground speed error 0.2 m s^{-1}	Ground speed error 0.5 m s^{-1}	Ground speed error 1.5 m s^{-1}
		True error/retrieved correction	
Tilt aft (°)	0.3/−0.271	0.3/−0.229	0.3/−0.090
Tilt fore (°)	−0.3/0.273	−0.3/0.233	−0.3/0.102
Rotation/roll aft (°)	1.0/−0.999	1.0/−0.999	1.0/−0.999
Rotation/roll fore (°)	2.0/−1.999	2.0/−1.999	2.0/−1.999
Pitch (°)	1.5/−1.487	1.5/−1.500	1.5/−1.500
Heading/drift (°)	0.5/−0.500	0.5/−0.500	0.5/−0.500
Range delay aft (m)	150/−150.0	150/−150.0	150/−150.0
Range delay fore (m)	200/−202.0	200/−202.0	200/−203.0
Δx (m)	—/—	—/—	—/—
Δy (m)	—/—	—/—	—/—
Δz (km)	0.3/−0.299	0.3/−0.298	0.3/−0.296
Ground speed (m s^{-1})	0.2/—	0.5/—	1.5/—
		Before → after correction	
Mean (STD) of DZ_{SURF} (km)	0.426 (0.183) → 0.000 (0.029)	0.426 (0.183) → 0.001 (0.029)	0.426 (0.183) → 0.000 (0.029)
Mean (STD) of V_{SURF} (m s^{-1})	1.928 (1.174) → −0.000 (0.000)	1.932 (1.141) → −0.001 (0.000)	1.943 (1.071) → −0.001 (0.000)

aircraft ground speed measurements improve with GPS technology.

c. *Test of GNCM under a moving surface condition*

One advantage of the GRH method over the THL method is its capability of utilizing aircraft in situ winds as a constraint to derive navigation corrections in airborne Doppler radar data. This capability is especially important for airborne Doppler radar data collected over a moving surface (i.e., ocean), where the THL method probably would fail as a result of violation of the still, flat surface assumption. Recognizing the limitations of the THL method, BLW developed a method that employed aircraft flight-level winds to deduce navigation corrections. Although the effectiveness of the BLW method has been demonstrated and used in several ELDORA field campaigns over the ocean [e.g., THORPEX Pacific Asian Regional Campaign (T-PARC)/Tropical Cyclone Structure 2008 (TCS08); Bell and Montgomery 2010], the algorithm itself is rather complicated to run and difficult to automate. Besides, the BLW method provides corrections only for tilt, drift, and ground speed; the other correction factors have to be obtained through the THL method. Therefore, the BLW method can be applied only over flat surfaces, just like the THL method.

We have shown in the previous section that a combination of cost functions J_1 and J_2, which represents the assumption of a nonmoving surface, is able to retrieve navigation errors reasonably well using synthetic ELDORA data. Now in this section we test how a combination of cost functions J_1 and J_3, which does not require a nonmoving surface assumption, would perform by using the same set of synthetic data. This kind of test was not done in the original paper by GRH, but we believe it warrants further investigation before the GNCM can be applied over a moving surface.

Three sets of ELDORA synthetic data that were used in the previous section (i.e., data with no tilt errors, no ground speed errors, and with both tilt and ground speed errors) were used to test the in situ cost function. These experiments are the same as in the previous section except that in situ cost function J_3 and surface height cost function J_1 are used in the retrieval instead of J_2 and J_1. Tests to determine the best range and elevation angle of the Doppler velocity near the aircraft to be used in the computation of the in situ cost function indicate that the derived corrections can be sensitive to range and elevations limits and could be case dependent. GRH's original recommendation was to restrict to <3 km in range and $<\pm5°$ in elevation, but it was found that a closer range and including more elevation angles yielded slightly better results for the synthetic data, while a longer range and fewer elevation angles yielded better results for other tests with real data (not shown). The tests suggest that the calculation depends on the variation of the actual wind field near the aircraft and that it can be sensitive to vertical and horizontal wind shear. Since the first few range gates are usually bad in real data as a result of saturation of the receiver, 1 km from the aircraft is about as close as possible. Therefore, we follow GRH's recommendation of using Doppler velocity data from low-elevation angles ($<\pm5°$) but limit the range of single-Doppler data to ~1 km instead of ~3 km

TABLE 4. True errors and retrieved navigation corrections using DTM and in situ cost functions for three sets of synthetic ELDORA data under the condition of a stationary surface. Also shown in the lower part of the table are the mean and STD of DZ_{SURF} and D_{IN_SITU} before and after the navigation correction was applied for the three sets of synthetic data.

	No tilt error	No ground speed error	With tilt and ground speed error
		True error/retrieved correction	
Tilt aft (°)	—/—	0.3/−0.205	0.3/−0.358
Tilt fore (°)	—/—	−0.3/0.093	−0.3/0.237
Rotation/roll aft (°)	1.0/−1.035	1.0/−1.035	1.0/−1.035
Rotation/roll fore (°)	2.0/−1.973	2.0/−1.973	2.0/−1.973
Pitch (°)	1.5/−1.517	1.5/−1.518	1.5/−1.517
Heading/drift (°)	0.5/−0.499	0.5/−0.503	0.5/−0.499
Range delay aft (m)	150/−151.0	150/−152.0	150/−152.0
Range delay fore (m)	200/−202.0	200/−201.0	200/−200.0
Δx (m)	—/—	—/—	—/—
Δy (m)	—/—	—/—	—/—
Δz (km)	0.3/−0.300	0.3/−0.297	0.3/−0.300
Ground speed ($m\,s^{-1}$)	1.0/−0.96	—/—	1.0/—
		Before → after correction	
Mean (STD) of DZ_{SURF} (km)	0.430 (0.183) → 0.000 (0.029)	0.426 (0.183) → −0.000 (0.029)	0.426 (0.183) → 0.000 (0.029)
Mean (STD) of D_{IN_SITU} ($m\,s^{-1}$)	0.103 (2.345) → 0.110 (0.542)	0.109 (2.392) → −0.001 (0.542)	0.101 (2.359) → 0.000 (0.542)

in the following tests. For real data cases, these limits can be adjusted slightly depending on the horizontal and vertical wind shear in the near environment by examining the Doppler velocity data near the aircraft.

The true errors and retrieved navigation corrections for tests with $J_1 + J_3$ are shown in the upper part of Table 4, with the reduction of mean and STD of surface height and Doppler velocity errors demonstrated in the lower part of Table 4. Notice the reduction of velocity error STD is much more prominent than its mean, because the mean error was very small from the beginning. Table 4 illustrates that cost function combination $J_1 + J_3$ was able to retrieve the navigation corrections with reasonable accuracy well within the accuracy of the algorithm itself, although the reduction of mean and STD of difference between in situ winds and Doppler velocity near the aircraft (i.e., D_{IN_SITU} in Table 4) was much less than the reduction of mean and STD of V_{SURF} (see Tables 1 and 2). For example, the mean (STD) of V_{SURF} reduced from ~1.9 (~1.1) $m\,s^{-1}$ to ~0.0 (~0.0) $m\,s^{-1}$ in Tables 1 and 2, where cost function combination $J_1 + J_2$ was used, while the mean (STD) of the difference between in situ wind and Doppler wind near the aircraft changed from only ~0.1 (~2.4) $m\,s^{-1}$ to ~0.0 (~0.5) $m\,s^{-1}$ in Table 4, where cost function combination $J_1 + J_3$ was used. Notice that even if the STD of D_{IN_SITU} is reduced by a factor of ~5 after the navigation corrections were applied, it is still nowhere close to the near-zero STD in Tables 1 and 2. As for the retrieval results of correction factors, when there is no tilt error in the synthetic data (column named "No tilt error" in Tables 1 and 4), all the retrieved correction factors were very close to each other between cost function combinations $J_1 + J_2$ and $J_1 + J_3$. For the case of "No ground speed error" in the synthetic data, cost function combination $J_1 + J_2$ (Table 1) slightly outperformed $J_1 + J_3$ (Table 4) in terms of tilt, while all other factors were all very accurately obtained. Finally, when both tilt and ground speed errors were included in the synthetic data and the ground speed error was ignored, cost function combination $J_1 + J_2$ (Table 2) slightly underperformed $J_1 + J_3$ (Table 4) in terms of tilt, while all other parameters were accurately retrieved. However, although there are differences in retrievals between using cost function combination $J_1 + J_2$ versus $J_1 + J_3$, they are within the accuracy of the GRH method established by GRH (i.e., 0.2° for angles). Thus, we can conclude that using $J_1 + J_2$ or $J_1 + J_3$ yields comparable retrieved results in terms of correction factors for synthetic data. But for practical reasons we will discuss later, using $J_1 + J_2$ is always recommended for real cases where the surface is stationary.

There are several limitations inherent in the in situ cost function formulation that makes the reduction of STD of D_{IN_SITU} close to zero almost impossible and the minimization process more difficult: 1) the variation of radar-measured winds along the radar beam near the aircraft, 2) the single-Doppler velocity measured along the radar beam near the aircraft versus the three-dimensional in situ wind field at the aircraft, and 3) the small initial averaged error of Doppler velocity compared to in situ winds (mean error of ~0.1 $m\,s^{-1}$ in Table 4) before navigation correction. In fact, GRH noted in their paper that the velocity error reduction by cost function J_3 was rather small because the magnitude of the initial velocity error was small to begin with in

TABLE 5. A list of ELDORA field projects.

No.	Year	Acronym	Surface	Reference
1	1993	TOGA COARE	Ocean	Webster and Lukas (1992)
2	1995	VORTEX-95	Flat land	Rasmussen et al. (1994)
3	1997	FASTEX	Ocean	Joly et al. (1997)
4	1998	Lake-ICE	Lake	Kristovich et al. (2000)
5	1999	MAP	Complex terrain	Bougeault et al. (2001)
6	2002	CRYSTAL-FACE	Land/Ocean	Jensen et al. (2004)
7	2002	IHOP	Flat land	Weckwerth et al. (2004)
8	2003	BAMEX	Flat land	Davis et al. (2004)
9	2005	RAINEX	Ocean	Houze et al. (2006)
10	2008	T-PARC	Ocean	Bell and Montgomery (2010)

their case as well. In contrast to velocity differences with in situ winds, the initial value of the averaged surface velocity errors was much larger (a mean of $\sim 1.9\,\mathrm{m\,s^{-1}}$ in Table 1) before the correction, which could make the minimization process easier. On the other hand, trying to minimize an error that is already small is numerically challenging for the algorithm, as in the case when cost function J_3 is utilized.

Although the tests of cost function J_3 using synthetic ELDORA data proved to be successful, it should be kept in mind that in a real-world case scenario, there might be challenges to apply this method. First, there is no error in both radar and in situ data from the synthetic dataset, which makes it possible to attribute the rather small in situ cost function values to navigation errors; second, there are no nonmeteorological data, such as second-trip echoes or sidelobes, in the synthetic radar data, which is certainly not true in real data. Although the latter error (i.e., nonweather echoes) is difficult to simulate in the synthetic data, the former error is fairly easy to add in the synthetic single-Doppler velocity. A few tests with white noise added to the Doppler velocity field were carried out. It was found that noise with zero bias and $1\,\mathrm{m\,s^{-1}}$ standard deviation does not change the retrieval results at all for both cost function combinations (i.e., $J_1 + J_2$ and $J_1 + J_3$), while noise with a positive bias of $0.5\,\mathrm{m\,s^{-1}}$ will increase the tilt correction errors by $\sim 0.248°$ and $\sim 0.268°$ for cost functions $J_1 + J_2$ and $J_1 + J_3$, respectively, for the synthetic dataset used in Table 4, column 3. All other correction factors remain more or less the same. Since the accuracy of this algorithm is $\sim 0.2°$ for angles, a velocity bias of $0.5\,\mathrm{m\,s^{-1}}$ is probably as large as can be tolerated.

In summary, the errors in single-Doppler velocity from radar, in situ wind measurement from airborne sensors, and erroneous data as a result of second-trip echoes, sidelobes, and low signal-to-noise ratios in real airborne Doppler radar data certainly will require extra caution when the GNCM is applied to real airborne Doppler radar data, especially when the in situ cost function is involved. The test of the GNCM in real-world case scenarios will be presented in the following section.

4. Test of the GNCM using real ELDORA data

In the previous section we showed the generalized navigation correction method performed satisfactorily for the synthetic ELDORA data within the accuracy of the algorithm as demonstrated in the original GRH paper. In this section we chose three datasets from three previous ELDORA field campaigns to test if the algorithm works in real ELDORA cases. As indicated in Table 5, out of a total of 10 field projects that ELDORA was involved in the past two decades or so, 5 of them (50%) were over water (4 over ocean plus 1 over lake), 3 of them (30%) were over flat land, 1 of them (10%) was over complex terrain, and 1 of them (10%) was over a land–ocean boundary. The three experiments selected in this study represent different surface conditions that an airborne Doppler radar could encounter. The first case, which is from the Bow Echo and Mesoscale Convective Vortex (MCV) Experiment (BAMEX; Davis et al. 2004), represents a case of a flat and still surface; the second case, which is from the Mesoscale Alpine Programme (MAP; Bougeault et al. 2001), represents a case of still and complex terrain; and finally, the third case, which is selected from T-PARC/TCS08 (Bell and Montgomery 2010), represents a case over flat ocean, where the surface velocity might not be zero. For the first two cases, a combination of surface height cost function J_1 and surface velocity cost function J_2 were applied; while in the third case, a combination of surface height cost function J_1 and in situ cost function J_3 were employed. All the legs used in the tests need to be at least ~ 5 min long, relatively straight and smooth (i.e., not very turbulent), and the aircraft has to be at a height not very close to ground ($\geq \sim 3$ km AGL for accurate retrieval of the rotation angle; THL). There are two possible reasons that turbulence might adversely affect the performance of any navigation correction algorithm.

TABLE 6. Retrieved navigation corrections for three cases from past field experiments (0252:00–0259:00 UTC 23 Jun 2003 during BAMEX, 1700:00–1715:00 UTC 15 Sep 1999 during MAP, and 0239:00–0249:00 UTC 22 Sep 2008 during T-PARC). Also shown in the lower part of the table are the mean and STD of DZ_{SURF}, V_{SURF}, and D_{IN_SITU} before and after the navigation correction was applied for the three cases.

	BAMEX	MAP	T-PARC
Tilt aft (°)	0.298	0.363	0.101
Tilt fore (°)	−0.295	0.010	−0.043
Rotation/roll aft (°)	−1.247	−2.556	−0.125
Rotation/roll fore (°)	−1.611	−3.220	−0.331
Pitch (°)	−1.424	−1.507	−1.791
Heading/drift (°)	0.098	−0.228	−0.502
Range delay aft (m)	117.0	105.0	184.0
Range delay fore (m)	110.0	85.0	158.0
Δx (m)	—	−764.0	—
Δy (m)	—	−788.0	—
Δz (km)	0.063	0.117	−0.017
Ground speed ($m\,s^{-1}$)	—	—	—
		Before → after correction	
Mean (STD) of DZ_{SURF} (km)	0.076 (0.155) → −0.000 (0.057)	0.109 (0.818) → 0.028 (0.322)	0.104 (0.069) → 0.000 (0.045)
Mean (STD) of V_{SURF} ($m\,s^{-1}$)	1.137 (0.954) → 0.001 (0.377)	1.164 (1.273) → −0.003 (0.697)	—
Mean (STD) of D_{IN_SITU} ($m\,s^{-1}$)	—	—	−0.218 (1.184) → −0.075 (1.152)

First, the momentum arm caused by the physical separation of aircraft INS and radar antenna when changes in aircraft altitude/pitch/heading are nonzero produces a Doppler velocity bias that can be estimated by knowing the time derivative of heading and pitch (dH/dt and dP/dt; see Lee et al. 1994). A second effect of turbulence is distortion of the airframe that introduces both Doppler velocity and beam position errors, which are rather difficult to quantify and thus can be treated only as random errors in a statistical sense. Quantitative critical values that can be used to exclude any turbulent legs for navigation correction purpose have yet to be found, which leads us to recommend that the calibration legs be flown in a straight and smooth pattern. This recommendation does not mean the algorithm will fail whenever there is turbulence, and it is quite possible that the GNCM might still work under light or even moderate turbulence, but this is difficult to test analytically.

For the BAMEX and MAP cases, the raw, unedited radar reflectivity and Doppler velocity were used in the retrievals because only surface echoes were necessary. However, the successful retrievals of navigation corrections for the T-PARC case need editing of the clear-air returns near the aircraft, because spurious echoes caused by sidelobes, second-trip echoes, and low signal-to-noise ratios have a tremendous effect on the performance of the algorithm. It is found that only after careful cleaning up of the clear-air returns near the aircraft does the in situ cost function J_3 function properly. This is not surprising, since the minimization of a cost function is prone to errors when the input data contain too much noise and have some bias.

It should be pointed out that sophisticated, automatic QC is not part of the GNCM algorithm, although simple editing using a threshold of spectrum width or normalized coherent power is included in the GNCM code. Therefore, a careful editing of Doppler data near the aircraft should first start with the automatic QC developed by Bell et al. (2013) with a "low" threshold to keep as much weather echo as possible, followed by a careful manual editing of all sweeps near the aircraft to ensure the Doppler velocity is free of noise.

The retrieved navigation corrections with the assumption of zero ground speed error for the three cases from BAMEX, MAP, and T-PARC are shown in the upper part of Table 6. The retrieved navigation corrections are within the normal range of values that we would expect based on past experiences. The effect of navigation correction is demonstrated in the lower part of Table 6 by the reduction of mean and STD between the difference of radar and DTM-derived surface height, surface velocity, as well as the difference between single-Doppler velocities and projected in situ winds on the radar beam near the aircraft (<1-km range) and at low elevation angles ($<\pm5°$). As an example, a sweep of single-Doppler velocity, which is approximately a vertical cross section from the MAP experiment at 1710 UTC 15 September 1999, is shown in Fig. 3 to demonstrate the effectiveness of navigation correction. Notice the velocity of surface echoes in Fig. 3b comes closer to zero in Fig. 3d (e.g., the gray inside the 35-dBZ radar reflectivity contour) after applying the correction factors. Also notice the small rotation between uncorrected and corrected radar

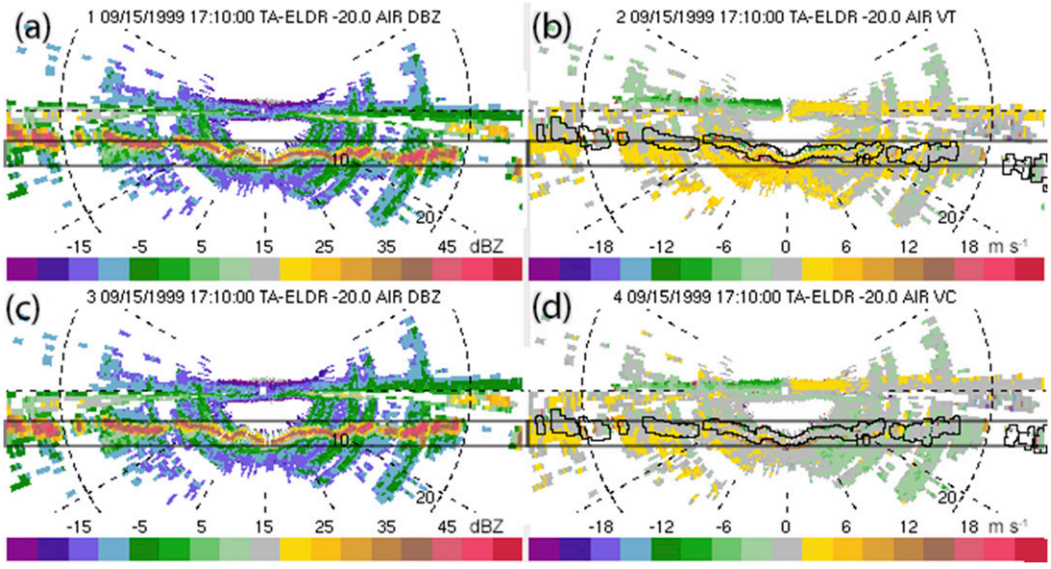

FIG. 3. An example of uncorrected vs corrected ELDORA reflectivity and single-Doppler velocity at 1710:00 UTC 15 Sep 1999 during MAP. (a) Uncorrected radar reflectivity, (b) uncorrected single-Doppler velocity, (c) corrected radar reflectivity, and (d) corrected single-Doppler velocity. Light black boxes in all four panels are used to show the horizon. Ground echoes over 35 dBZ in (b) and (d) are drawn as thin black contours.

reflectivity (Figs. 3a and 3c) and the Doppler velocity field (Figs. 3b and 3d). The difference in Doppler velocity from applying the corrections is shown in Fig. 4. The correction is range and azimuth dependent and has a maximum magnitude of $\sim 4\,\mathrm{m\,s^{-1}}$.

Similar to conclusions drawn from using synthetic ELDORA data in the previous section, the effectiveness of using cost function J_2 for the velocity constraint can be seen when the mean (STD) of V_{SURF} in Table 6 changed from 1.137 (0.954) $\mathrm{m\,s^{-1}}$ to 0.001 (0.377) $\mathrm{m\,s^{-1}}$ for the BAMEX case and from 1.164 (1.273) $\mathrm{m\,s^{-1}}$ to -0.003 (0.697) $\mathrm{m\,s^{-1}}$ for the MAP case after the retrieved correction factors were applied. The smaller reduction of STD of V_{SURF} in MAP is a result of complex terrain as pointed out by GRH. As for the T-PARC case where cost function J_3 was employed instead of cost function J_2 for the velocity constraint, the mean (STD) of $D_{\mathrm{IN\_SITU}}$ in Table 6 changed from -0.218 (1.184) $\mathrm{m\,s^{-1}}$ to -0.075 (1.152) $\mathrm{m\,s^{-1}}$. Notice the STD of $D_{\mathrm{IN\_SITU}}$ did not decrease much after correction although the mean of $D_{\mathrm{IN\_SITU}}$ did reduce to near zero.

Last, we compare the results of the GNCM with published correction factors for a calibration leg from the 1995 VORTEX (VORTEX-95; Rasmussen et al. 1994) field experiment described in BLW in Table 7. The VORTEX-95 case provides a unique reference case where correction factors using the THL, BLW, and GNCM $J_1 + J_2$ and $J_1 + J_3$ methods can all be compared because of extensive near-aircraft echoes and a flat, nonmoving surface. By calculating the $J_1 + J_3$ in a case with a stationary surface, we can directly compare how the GNCM performs without the surface velocity constraint against the BLW and THL reference solutions, which are not both available in overocean cases. The corrections are very similar, with the largest discrepancy found using the $J_1 + J_3$ cost function. The differences between THL, BLW, and the $J_1 + J_2$ methods are very small and within the standard deviations of the THL uncertainty presented in BLW (see their Table 6), with the exception of the aft tilt correction, which is 0.3° larger. This discrepancy is likely due to the assumption of zero ground speed error, which is estimated to be near $1.0\,\mathrm{m\,s^{-1}}$. The results using $J_1 + J_3$ are quantitatively similar, but with slightly larger tilt, a smaller rotation angle, and smaller pitch corrections. If the BLW correction is considered to be closest to a ''reference''

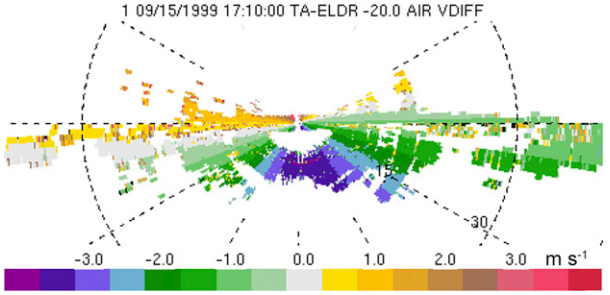

FIG. 4. The difference field ($\mathrm{m\,s^{-1}}$) between the corrected and uncorrected single-Doppler velocity at 1710:00 UTC 15 Sep 1999 during MAP.

TABLE 7. Retrieved navigation corrections for three methods from the 0057 UTC 8 May 1995 VORTEX-95 flight leg. THL and BLW results are from Table 3 in BLW.

	THL	BLW	GNCM $J_1 + J_2$	GNCM $J_1 + J_3$
Tilt aft (°)	0.3	0.2	0.5	0.8
Tilt fore (°)	−0.2	−0.3	−0.2	−0.7
Rotation/roll aft (°)	−1.1	−1.1	−1.1	−0.8
Rotation/roll fore (°)	2.7	2.7	2.7	2.5
Pitch (°)	−1.5	−1.4	−1.4	−1.7
Heading/drift (°)	−0.2	−0.1	0.0	0.0
Range delay aft (m)	170.0	170.0	155.0	158.0
Range delay fore (m)	175.0	175.0	139.0	147.0
Δx (m)	—	—	—	—
Δy (m)	—	—	—	—
Δz (km)	0.055	0.055	−0.016	−0.010
Ground speed ($m\,s^{-1}$)	0.8	1.0	—	—

solution, then the $J_1 + J_2$ solution can be considered superior to the $J_1 + J_3$ solution, but both sets of navigation corrections produce very similar dual-Doppler wind fields without the need for the more complicated BLW procedure. These results further confirm the effectiveness of the GNCM using real data that gives comparable results to the well-established BLW and THL correction methods. The results also reaffirm that while $J_1 + J_3$ can yield satisfactory results, the $J_1 + J_2$ cost function is recommended if the nonmoving surface constraint is applicable.

5. Summary and discussion

A generalized navigation correction method (GNCM) to retrieve airborne Doppler radar navigation errors for all surface conditions is presented. The algorithm is based on GRH and has the following improvements compared with the original GRH method: 1) tilt corrections for both fore and aft antennas are added and 2) roll/rotation corrections for fore and aft antennas are separated. The effectiveness of the GNCM is fully tested using synthetic ELDORA data with prespecified navigation errors. The tests confirmed a previous finding by THL that tilt, drift/heading, and aircraft ground speed errors form an underdetermined system; therefore, closure assumptions have to be made to retrieve these three errors. Unlike THL and the original GRH method, which assumed zero tilt error, we propose to assume a zero ground speed error, which is novel. Under the zero ground speed error assumption, the method can accurately retrieve the other navigation corrections, including tilt correction, even with small actual ground speed errors. Given the recent improvements in GPS technology, the actual ground speed error is expected to be very small and to continue to decrease in the future.

Another focus of this paper, which was not adequately addressed in GRH, is the test of the effectiveness of in situ cost function J_3. In the original GRH method, the surface height cost function J_1, the surface velocity cost function J_2, and the in situ-cost function J_3 were all used in the retrievals of navigation corrections. Since both cost functions J_2 and J_3 provide velocity constraints in the algorithm, it is not necessary to include the in situ cost function J_3 for airborne Doppler radar navigation correction over a stationary surface. On the other hand, for navigation correction over a moving surface, the surface velocity cost function J_2 cannot be applied and the in situ cost function has to be included. Tests using synthetic ELDORA data suggest that the cost function combinations $J_1 + J_2$ and $J_1 + J_3$ provide satisfactory correction factors within the accuracy of the algorithm that was established by GRH, although in real cases it is always recommended that $J_1 + J_2$ be used for stationary surface because the potential data quality and representativeness issues associated with the Doppler velocities near the aircraft.

Another finding of this paper based on multiple tests of the in situ cost function J_3 using different thresholds of distance from the aircraft and different elevation angles of radar beams in different cases is that the algorithm can be sensitive to variations in the local wind field caused by horizontal and vertical winds shear. The tests indicate that using data from close range (<1 km) and low-elevation angles ($<\pm5°$) is best as a general recommendation, but these limits can be more or less restrictive depending on the specific wind field near the radar along the calibration leg.

Tests of the GNCM using real ELDORA data collected from previous field projects were also performed. Satisfactory results were readily obtained using raw ELDORA data for cases over still surfaces with complex terrain (e.g., data from MAP), or flat terrain (e.g., data from BAMEX). However, for cases over ocean, where the surface velocity cannot be assumed to be zero, the usage of the in situ cost function J_3 is necessary and

needs careful consideration. First of all, there must be enough radar returns near the aircraft so that enough data points can be identified for calculation of cost function J_3. Second, and probably most importantly, the radar data near the aircraft have to be edited properly so that spurious second-trip echoes, sidelobes, and low signal-to-noise ratios will not be included in the calculation. This requirement warrants an automatic data quality control algorithm for airborne Doppler radar data, such as the algorithm using Solo (Oye et al. 1995) described by Bell et al. (2013). Tests using T-PARC data showed that the in situ cost function could perform properly only after cleanup of radar data near the aircraft.

One other possible failure mode of the algorithm is when it has trouble identifying surface echoes correctly. Since the method uses radar reflectivity and the gradient of radar reflectivity along a radar beam to find surface echoes, it might have trouble properly identifying surface echoes when a strong storm extends all the way to the ground near the aircraft. Normally surface echoes would have single-Doppler velocity close to zero and surface height close to DTM-derived height, while weather echoes do not necessarily have near-zero velocity close to DTM-derived heights. Fortunately, this kind of problem is fairly easy to identify, since the algorithm will produce outrageous values for navigation correction factors when weather echoes are mistakenly identified as surface echoes. However, this contingency needs to be recognized by the user.

In summary, in this paper we have 1) developed a generalized navigation correction method that works in all surface conditions (stationary or moving, flat or complex) with the tilt correction, 2) proposed a new closure assumption (zero ground speed error) based on improved GPS technology and theoretical considerations, and 3) evaluated the algorithm thoroughly in a variety of circumstances using both synthetic and real ELDORA data. In addition, the formulation of the generalized algorithm is independent of platforms; therefore, it has the potential of becoming a single algorithm for all future airborne Doppler radar navigation correction needs.

Acknowledgments. This research is partially funded by American Recovery and Reinvestment Act. The first author was also partially funded by the U.S. Army Research Laboratory. MMB and WCL were supported under National Science Foundation SI2-SSI Award ACI-1661663. MMB was also supported by the Office of Naval Research Award N000141613033. The National Center for Atmospheric Research is sponsored by the National Science Foundation. Constructive comments from three anonymous reviewers greatly improved this paper. Their help is greatly appreciated.

APPENDIX A

Parameter List for GNCM

x_{RAD}, y_{RAD}, z_{RAD}	Radar-derived x, y, and z, respectively, in the Earth-relative coordinate system
Δx, Δy, Δz	Corrections of x_{RAD}, y_{RAD}, z_{RAD}, respectively
n	nth element of an array
h_{DTM}	DTM-derived surface height
N_{SURF}	Total number of surface gates
μ_{SURF}	Weight of surface gates
V_{SURF}	Doppler velocity of surface gates
N_{NEAR}	Total number of gates close to radar and at low-elevation angles
μ_{NEAR}	Weight of gates close to radar and at low-elevation angles
V_{NEAR}	Doppler velocity of the gates close to radar and at low-elevation angles
P, ΔP	Pitch angle and its correction, respectively
H, ΔH	Heading angle and its correction, respectively
d_f, Δd_f	Radar range delay and its correction for the fore antenna, respectively
d_a, Δd_a	Radar range delay and its correction for the aft antenna, respectively
T_f, ΔT_f	Tilt angle and its correction for the fore antenna, respectively
T_a, ΔT_a	Tilt and its correction for the aft antenna, respectively
R_f, ΔR_f	Rotation angle and its correction for the fore antenna, respectively
R_a, ΔR_a	Rotation and its correction for the aft antenna, respectively
ΔV	Aircraft ground speed correction
J_1, J_2, and J_3	Surface height, surface velocity, and in situ wind cost function, respectively
δ_1, δ_2, and δ_3	On/off switch (0 or 1) for cost functions J_1, J_2, and J_3, respectively
J	The total cost function, which is the normalized sum of $\delta_1 J_1 + \delta_2 J_2 + \delta_3 J_3$

APPENDIX B

Synthetic Radar Dataset

This appendix provides a brief description of the synthetic radar dataset used for testing Doppler wind retrieval techniques. The wind field is composed of a three-dimensional Beltrami flow of alternating counterrotating vortices and updrafts. The wind field satisfies mass continuity and is of a class of exact

solutions to the incompressible Navier–Stokes equations. The flow is designed to qualitatively resemble a field of deep moist cyclonic convective towers surrounded by anticyclonic downdrafts. This particular wind field was used by Shapiro (1993) to test and validate the ARPS nonhydrostatic model, and by Shapiro et al. (2009) to test a Doppler wind retrieval technique. The analytic wind field is given by

$$u = U - \frac{A}{k^2 + l^2}\{\Lambda l \cos[k(x - Ut)]\sin[l(y - Vt)]\sin(mz) + mk\sin[k(x - Ut)]\cos[l(y - Vt)]\cos(mz)\}\exp(-\upsilon\Lambda^2 t) \tag{B1a}$$

$$\upsilon = V + \frac{A}{k^2 + l^2}\{\Lambda k \sin[k(x - Ut)]\cos[l(y - Vt)]\sin(mz) - ml\cos[k(x - Ut)]\sin[l(y - Vt)]\cos(mz)\}\exp(-\upsilon\Lambda^2 t) \tag{B1b}$$

$$w = A\cos[k(x - Ut)]\cos[l(y - Vt)]\sin(mz) \times \exp(-\upsilon\Lambda^2 t). \tag{B1c}$$

The parameters used for this study were

$$A = U = V = 10\,\mathrm{m\,s^{-1}}, \quad m = 2\pi/(32\,\mathrm{km}), \quad k = l = 2\pi/(16\,\mathrm{km}), \quad \text{and} \quad \Lambda = 0.$$

ELDORA was virtually flown on a straight and level south–north track ~35 km long and sampled the analytic wind field defined by a Cartesian coordinate system centered at 16.5°N and 148°E. This is the approximate location of the T-PARC/TCS08 dataset used for validation of automatic quality control procedures by Bell et al. (2013) but was otherwise arbitrary. The sampled reflectivity of the analytic wind field is given by

$$\mathrm{dB}Z = 45\cos\{k[x - Ut]\cos[l(y - Vt)] \times \cos[m(z - 1000)/2\}, \tag{B2}$$

above the surface. This reflectivity distribution yields high reflectivity columns in the updraft regions and low reflectivity columns in the downdraft regions. The distribution provides a reasonable way to mimic the effect of deep convective echoes near the surface that could impact the navigation correction algorithm. The terminal fall speed of hydrometeors was neglected for this application.

The radar beam was modeled as a rectangular beam with a 1.8° circular beamwidth with an identical rotation rate of ELDORA. The average radial velocity and reflectivity at each range gate were obtained by subsampling the beam solid angle in small spherical coordinate increments centered at the beam axis. Individual "pulses" were therefore obtained from discrete spatial locations within the beam as opposed to temporal sampling of the entire radar volume. Pulses sampling the surface were given a zero radial velocity and 50-dBZ reflectivity. The final radial velocity was the power-weighted average of the individual pulses. Inertial navigation system errors were added to the aircraft data depending on the specific tests described in the text.

REFERENCES

Bell, M. M., and M. T. Montgomery, 2010: Sheared deep vortical convection in pre-depression Hagupit during TCS08. *Geophys. Res. Lett.*, **37**, L06802, https://doi.org/10.1029/2009GL042313.

——, W.-C. Lee, C. A. Wolff, and H. Cai, 2013: A Solo-based automated quality control algorithm for airborne tail Doppler radar data. *J. Appl. Meteor. Climatol.*, **52**, 2509–2528, https://doi.org/10.1175/JAMC-D-12-0283.1.

Bosart, B. L., W.-C. Lee, and R. M. Wakimoto, 2002: Procedures to improve the accuracy of airborne Doppler radar data. *J. Atmos. Oceanic Technol.*, **19**, 322–339, https://doi.org/10.1175/1520-0426-19.3.322.

Bougeault, P., and Coauthors, 2001: The MAP special observing period. *Bull. Amer. Meteor. Soc.*, **82**, 433–462, https://doi.org/10.1175/1520-0477(2001)082<0433:TMSOP>2.3.CO;2.

Cai, H., and W. C. Lee, 2013: Observations of the 9 June dryline during IHOP. *Open Atmos. Sci. J.*, **7**, 77–91, https://doi.org/10.2174/1874282320130417002.

——, ——, T. M. Weckwerth, C. Flamant, and H. V. Murphey, 2006: Observations of the 11 June dryline during IHOP_2002—A null case for convection initiation. *Mon. Wea. Rev.*, **134**, 336–354, https://doi.org/10.1175/MWR2998.1.

Chong, M., and O. Bousquet, 1999: A mesovortex within a near-equatorial mesoscale convective system during TOGA COARE. *Mon. Wea. Rev.*, **127**, 1145–1156, https://doi.org/10.1175/1520-0493(1999)127<1145:AMWANE>2.0.CO;2.

Davis, C., and Coauthors, 2004: The Bow Echo and MCV Experiment: Observations and opportunities. *Bull. Amer. Meteor. Soc.*, **85**, 1075–1093, https://doi.org/10.1175/BAMS-85-8-1075.

Georgis, J. F., F. Roux, and P. H. Hildebrand, 2000: Observation of precipitating systems over complex orography with meteorological Doppler radars: A feasibility study. *Meteor. Atmos. Phys.*, **72**, 185–202, https://doi.org/10.1007/s007030050015.

Guy, N., and D. P. Jorgensen, 2014: Kinematic and precipitation characteristics of convective systems observed by airborne Doppler radar during the life cycle of a Madden–Julian oscillation in the Indian Ocean. *Mon. Wea. Rev.*, **142**, 1385–1402, https://doi.org/10.1175/MWR-D-13-00252.1.

Hildebrand, P. H., and Coauthors, 1996: The ELDORA/ASTRAIA airborne Doppler weather radar: High-resolution observations from TOGA COARE. *Bull. Amer. Meteor. Soc.*, **77**, 213–232, https://doi.org/10.1175/1520-0477(1996)077<0213:TEADWR>2.0.CO;2.

Houze, R. A., Jr., and Coauthors, 2006: The Hurricane Rainband and Intensity Change Experiment: Observations and modeling of Hurricanes Katrina, Ophelia, and Rita. *Bull. Amer. Meteor. Soc.*, **87**, 1503–1521, https://doi.org/10.1175/BAMS-87-11-1503.

Jensen, E., D. Starr, and B. Toon, 2004: Mission investigates tropical cirrus clouds. *Eos, Trans. Amer. Geophys. Union*, **85**, 45–50, https://doi.org/10.1029/2004EO050002.

Joly, A., and Coauthors, 1997: The Fronts and Atlantic Storm-Track Experiment (FASTEX): Scientific objectives and experimental design. *Bull. Amer. Meteor. Soc.*, **78**, 1917–1940, https://doi.org/10.1175/1520-0477(1997)078<1917:TFAAST>2.0.CO;2.

Jorgensen, D. P., M. A. LeMone, and S. B. Trier, 1997: Structure and evolution of the 22 February 1993 TOGA COARE squall line: Aircraft observations of precipitation, circulation, and surface energy flux. *J. Atmos. Sci.*, **54**, 1961–1985, https://doi.org/10.1175/1520-0469(1997)054<1961:SAEOTF>2.0.CO;2.

Kristovich, D. A. R., and Coauthors, 2000: The Lake-Induced Convection Experiment and the Snowband Dynamics Project. *Bull. Amer. Meteor. Soc.*, **81**, 519–542, https://doi.org/10.1175/1520-0477(2000)081<0519:TLCEAT>2.3.CO;2.

Lee, W.-C., P. Dodge, F. D. Marks Jr., and P. H. Hildebrand, 1994: Mapping of airborne Doppler radar data. *J. Atmos. Oceanic Technol.*, **11**, 572–578, https://doi.org/10.1175/1520-0426(1994)011<0572:MOADRD>2.0.CO;2.

——, F. D. Marks Jr., and C. Walther, 2003: Airborne Doppler Radar Data Analysis Workshop. *Bull. Amer. Meteor. Soc.*, **84**, 1063–1075, https://doi.org/10.1175/BAMS-84-8-1063.

Marks, F. D., Jr., R. A. Houze Jr., and J. F. Gamache, 1992: Dual-aircraft investigation of the inner core of Hurricane Norbert. Part I: Kinematic structure. *J. Atmos. Sci.*, **49**, 919–942, https://doi.org/10.1175/1520-0469(1992)049<0919:DAIOTI>2.0.CO;2.

Oye, R., C. Mueller, and S. Smith, 1995: Software for radar translation, visualization, editing, and interpolation. Preprints, *27th Conf. on radar Meteorology*, Vail, CO, Amer. Meteor. Soc., 359–361.

Rasmussen, E. N., J. M. Straka, R. Davies-Jones, C. A. Doswell III, F. H. Carr, M. D. Eilts, and D. R. MacGorman, 1994: Verification of the Origins of Rotation in Tornadoes Experiment: VORTEX. *Bull. Amer. Meteor. Soc.*, **75**, 995–1006, https://doi.org/10.1175/1520-0477(1994)075<0995:VOTOOR>2.0.CO;2.

Reasor, P. D., M. D. Eastin, and J. F. Gamache, 2009: Rapidly intensifying Hurricane Guillermo (1997). Part I: Low-wavenumber structure and evolution. *Mon. Wea. Rev.*, **137**, 603–631, https://doi.org/10.1175/2008MWR2487.1.

Shapiro, A., 1993: The use of an exact solution of the Navier–Stokes equations in a validation test of a three-dimensional nonhydrostatic numerical model. *Mon. Wea. Rev.*, **121**, 2420–2425, https://doi.org/10.1175/1520-0493(1993)121<2420:TUOAES>2.0.CO;2.

——, C. K. Potvin, and J. Gao, 2009: Use of vertical vorticity equation in variational dual-Doppler wind analysis. *J. Atmos. Oceanic Technol.*, **26**, 2089–2106, https://doi.org/10.1175/2009JTECHA1256.1.

Tang, X., W.-C. Lee, and M. Bell, 2014: A squall-line-like principal rainband in Typhoon Hagupit (2008) observed by airborne Doppler radar. *J. Atmos. Sci.*, **71**, 2733–2746, https://doi.org/10.1175/JAS-D-13-0307.1.

Testud, J., P. H. Hildebrand, and W.-C. Lee, 1995: A procedure to correct airborne Doppler radar data for navigation errors using the echo returned from the earth's surface. *J. Atmos. Oceanic Technol.*, **12**, 800–820, https://doi.org/10.1175/1520-0426(1995)012<0800:APTCAD>2.0.CO;2.

Wakimoto, R. M., and B. L. Bosart, 2001: Airborne observations of a warm front during FASTEX. *Mon. Wea. Rev.*, **129**, 254–274, https://doi.org/10.1175/1520-0493(2001)129<0254:AROOAW>2.0.CO;2.

——, and H. Cai, 2002: Airborne observations of a front in a deformation zone during FASTEX. *Mon. Wea. Rev.*, **130**, 1898–1912, https://doi.org/10.1175/1520-0493(2002)130<1898:AOOAFN>2.0.CO;2.

——, and H. V. Murphey, 2009: Analysis of a dryline during IHOP: Implications for convection initiation. *Mon. Wea. Rev.*, **137**, 912–936, https://doi.org/10.1175/2008MWR2584.1.

——, C. Liu, and H. Cai, 1998: The Garden City, Kansas, storm during the VORTEX 95. Part I: Overview of the storm's lifecycle and mesocyclogenesis. *Mon. Wea. Rev.*, **126**, 372–392, https://doi.org/10.1175/1520-0493(1998)126<0372:TGCKSD>2.0.CO;2.

——, H. V. Murphey, and H. Cai, 2004: The San Angelo, Texas, supercell of 31 May 1995: Visual observations and tornadogenesis. *Mon. Wea. Rev.*, **132**, 1269–1293, https://doi.org/10.1175/1520-0493(2004)132<1269:TSATSO>2.0.CO;2.

Webster, P. J., and R. Lukas, 1992: TOGA COARE: The Coupled Ocean–Atmosphere Response Experiment. *Bull. Amer. Meteor. Soc.*, **73**, 1377–1416, https://doi.org/10.1175/1520-0477(1992)073<1377:TCTCOR>2.0.CO;2.

Weckwerth, T. M., and Coauthors, 2004: An overview of the International H_2O Project (IHOP_2002) and some preliminary highlights. *Bull. Amer. Meteor. Soc.*, **85**, 253–277, https://doi.org/10.1175/BAMS-85-2-253.